

Characterization of metal (Fe, Co, Ni, Cu) and fluorine codoped barium strontium titanate thick-films for microwave applications

Xianghui Zhou · Holger Geßwein · Mohsen Sazegar ·
Andre Giere · Florian Paul · Rolf Jakoby ·
Joachim R. Binder · Jürgen Haußelt

Received: 19 December 2008 / Accepted: 19 May 2009 / Published online: 30 May 2009
© Springer Science + Business Media, LLC 2009

Abstract The influence of codoping of Fe, Co, Ni, Cu as acceptors and F as donor on the dielectric properties of screen-printed $\text{Ba}_{0.6}\text{Sr}_{0.4}\text{TiO}_3$ ceramic thick-films has been investigated. The undoped and codoped $\text{Ba}_{0.6}\text{Sr}_{0.4}\text{TiO}_3$ powders were synthesized through a sol-gel route. The thermal gravimetric analysis revealed the difference of the thermal decomposition behaviour between the undoped and codoped precursors. The ceramic powders were characterized with x-ray diffraction, scanning electron microscopy and BET measurements. Larger crystallite sizes of the codoped powders were observed. The densification behaviour of the powders was recorded by dilatometry and indicated that codoping influences the sintering mechanism. The permittivity, dielectric loss and tunability of the undoped and codoped thick-films were characterized with coplanar waveguide structures up to 30 GHz.

Keywords BST · Codoping · Thick-film · Dielectric properties · Tunability · Microwave frequency

1 Introduction

Barium strontium titanates (BST) are promising candidates for applications in tunable microwave devices. Such devices include phase shifters, tunable matching networks, tunable filters, tunable antennas, as well as frequency agile oscillators and modulators [1–7]. The tuning of the different devices using BST is based on the large field dependence of the dielectric permittivity, which results in a passively tuning of the capacitance or phase velocity in the device, allowing it to be adjusted in real time for a particular application [8]. These devices can be realized on screen-printed BST thick-films on alumina substrates and allow to scale the tuning voltages and device linearity in regards to the applications requirement [6]. But the relatively high dielectric losses of the BST thick-films, especially at microwave frequencies, have precluded their use. It is well documented that small amounts of doping materials such as Mg, Mn, Fe, Co and Ni can remarkably reduce the dielectric losses of BST [9–15], but the tunability of BST is also lowered at the same time [9, 13–15]. Paul [13] has reported that Fe-F codoped BST thick-films show not only reduced dielectric losses, but also a higher tunability compared to the undoped thick-films at 10 kHz and ambient temperature.

In this study, we investigated the effects of acceptor-donor-codoping with Fe, Co, Ni, Cu as acceptor-dopants and F as donor-dopant. The dielectric

X. Zhou (✉) · H. Geßwein · J. R. Binder · J. Haußelt
Institute for Materials Research III,
Forschungszentrum Karlsruhe GmbH,
Hermann-von-Helmholtz-Platz 1,
76344 Eggenstein-Leopoldshafen, Germany
e-mail: Xianghui.Zhou@imf.fzk.de

X. Zhou · M. Sazegar · A. Giere · R. Jakoby
Microwave Engineering,
Darmstadt University of Technology,
Merckstrasse 25, 64283 Darmstadt, Germany

F. Paul · J. Haußelt
Institute of Microsystems Engineering,
University of Freiburg, Georges-Koehler-Allee 102,
79110 Freiburg, Germany

constants, dielectric losses and tunabilities of the codoped BST thick-films were characterized by coplanar waveguides (CPW) at microwave frequencies.

2 Experimental

Undoped and doped barium strontium titanate powders were synthesized through a modified sol-gel process. According to the empirical formula $\text{Ba}_{0.6}\text{Sr}_{0.4}\text{Ti}_{0.99}\text{Me}_{0.01}\text{O}_{3-x}\text{F}_{0.09}$ (Me=Fe, Co, Ni, Cu), the nominal compositions of all the prepared ceramic powders are listed in Table 1. Barium acetate ($\text{Ba}(\text{CH}_3\text{COO})_2$), strontium acetate ($\text{Sr}(\text{CH}_3\text{COO})_2$) and titanium-(IV)-isopropoxide ($\text{Ti}(\text{OCH}(\text{CH}_3)_2)_4$) were used as starting materials. Acetic acid was selected as solvent. Barium acetate and strontium acetate were initially dissolved in acetic acid and stirred over night at room temperature. The titanium-(IV)-isopropoxide was added in the solution under vigorous stirring. An exothermic reaction occurred and the temperature rose to approximately 30°C. In case of doped powders, the trifluoroacetic acid (TFA, CF_3COOH) was dropped in the acetic acid before the addition of titanium-(IV)-isopropoxide and the dopant with metal element was added into the clear and colorless solution after the exothermic reaction. After the solution was diluted with ultrapure water it was spray-dried. The spray-dried metal-organic precursor was calcined in alumina crucibles in a tube furnace under dried purified (molecular sieve and silica gel) air at 900°C for 1 h. Screen-printing pastes were prepared with calcined BST powder, vehicle and dispersant and were finally printed on polycrystalline alumina substrates (Rubalit710, CeramTec). In order to avoid crack formation during drying, screen-printed thick-films were cold isostatically densified (CIP) at 400 MPa before sintering. Finally, the thick-films were sintered in a tube furnace under dried purified air at 1200°C for 1 h with a heating rate and cooling rate of 5°C/min respectively.

The pyrolysis of the precursors was investigated by thermogravimetric analysis in a Netzsch STA 449C

thermal analyzer in air up to temperatures of 1200°C with a heating rate of 10°C/min. The sintering behaviour of the BST powders was studied by dilatometry (Netzsch DIL 402C) by heating uniaxially pressed powder compacts in flowing air at 5°C/min up to 1450°C. The chemical composition of the powders was measured using x-ray fluorescence spectroscopy (XRF, Bruker-AXS, SRS 303AS) and titration after hydro pyrolysis (laboratory of H.C. Starck GmbH, Goslar). In order to evaluate the fluorine concentration in the thick-films after sintering, small amounts of the corresponding screen-printing pastes were calcined according to the sintering conditions of the thick-films, i.e. in the tube furnace under dried purified air at 1200°C for 1 h, with a heating and cooling rate of 5°C/min. The concentration of fluorine in the calcined pastes was also measured using titration after hydro pyrolysis as described above. The BET surface was determined with a Micromeritics FlowSorb II 2300. The crystallographic structure of BST powders and thick-films was analyzed using x-ray diffraction (Siemens D5005, $\text{Cu } K_\alpha$ radiation). The morphology of the powders and thick-films was investigated via scanning electron microscopy (Zeiss Supra 55).

For the characterization of the tuning field dependent permittivity coplanar waveguide (CPW) structures were realized on top of the BST thick-films. The metallization of the CPW was processed by a single lithography step on a Cr/Au evaporated seed layer and strengthened by an Au galvanic step. The transmission line characteristics of the CPWs, which are dependent on tuning voltage, were determined by temperature controlled on-wafer S-parameter measurements using a vector network analyzer and sweeping the tuning voltage in a range from 0 V to 100 V. From the transmission line the complex capacitance per unit-length was computed using an inductance per unit-length calculated by Conformal Mapping (CM) methods. Based on the remaining complex capacitance value, the permittivity of the BST film was extracted using the iterative characterization method using a 2D-Finite-Difference Time-Domain method (2D-FDTD) based electromagnetic field solver adapted to the nonlinear material [16]. This

Table 1 Nominal compositions of the prepared ceramic powders and used dopants.

Sample name	Nominal molar composition relative to BST							
	Ba	Sr	Ti	Fe	Co	Ni	Cu	F
Undoped	0.60	0.40	1.00	–	–	–	–	–
Fe–F codoped	0.60	0.40	0.99	0.01	–	–	–	0.09
Co–F codoped	0.60	0.40	0.99	–	0.01	–	–	0.09
Ni–F codoped	0.60	0.40	0.99	–	–	0.01	–	0.09
Cu–F codoped	0.60	0.40	0.99	–	–	–	0.01	0.09

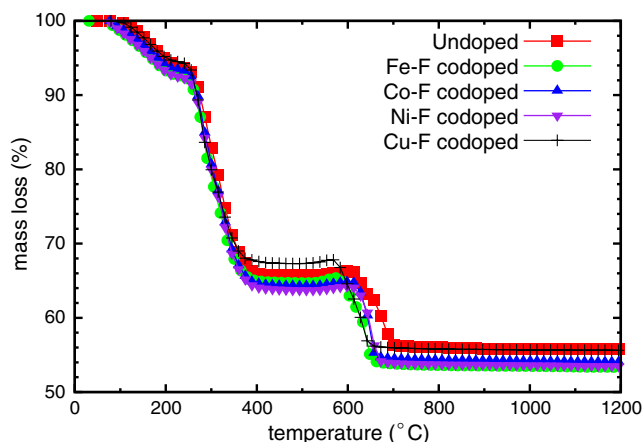


Fig. 1 TG curves of the undoped and codoped BST precursors recorded with a heating rate of 10°C/min under flowing synthetic air (20.5% O₂ in N₂, 100 ml/min)

method considers the inhomogeneous tuning field distribution in the BST thick-film and further the related inhomogeneous tuned permittivity.

3 Results and discussions

3.1 Characterization of BST powders

Thermal gravimetric analysis The TG curves of undoped and doped BST precursors heated from ambient temperature up to 1200°C are shown in Fig. 1. The TG curves of undoped as well as doped BST indicate that there are three apparent decreases in sample weight, which coincide with the decomposition behaviours of barium-titanium acetate gel precursors [17] and BST gel precursors [18–20] described in the literature. The first step begins at 100°C and ends at 220°C. This step can be explained with the vaporization of water and acetic acid which remained in the precursor after spray-drying. This corresponds to a weight loss of 6–8% in the TG curve. The second step ranges between 250 and 400°C and corresponds to a weight loss of about

36–45%. Referring to the literature, the metallorganic precursor turns to metastable oxycarbonate as an intermediate phase in this step with the combustion of decomposition products. The third step starts at approximately 550°C and ends at 650°C with a weight loss of about 9–12%. It is believed that in this region the metastable oxycarbonate decomposes to barium strontium titanate accompanied by its crystallization. As shown in Fig. 1, the dopants have a slight influence on the thermal decomposition of BST acetate gel precursors. The weight loss of the second step of the Cu-F codoped BST precursor is lower than that of the undoped precursors, while the other codoped BST precursors show higher weight losses compared to the undoped precursor. Furthermore the third step of the decomposition reaction of the codoped BST precursors, in which the intermediate phase converts to BST, takes place at lower temperatures compared to the undoped BST precursor. This is most pronounced for the Fe–F codoped and Cu–F codoped precursors.

X-ray powder diffraction and microstructure Phase composition and crystallinity of the calcined powders were investigated by means of powder x-ray diffraction. The x-ray patterns were refined with the Rietveld method using the *Fullprof* program [21]. As a profile function the TCH-pseudo-Voigt function was chosen. To account for the instrumental contribution to the peak broadening annealed BaF₂ powder was used as a standard line profile material. Rietveld refinements were undertaken based on cubic Ba_{0.6}Sr_{0.4}TiO₃ with space group (SG) *Pm* $\bar{3}$ *m* orthorhombic (Ba,Sr)CO₃ (SG *Pm**cn*) or cubic (Ba,Sr)F₂ (SG *Fm* $\bar{3}$ *m*). Microstructural parameters were extracted from the Rietveld refinements as described in [22]. Lattice parameters, the apparent volume-weighted size ϵ_β and upper-limit (maximum) microstrain values ϵ obtained by the Rietveld refinements are listed in Table 2 and the measured x-ray patterns are shown in Fig. 2. Small amounts of residual (Ba,Sr)CO₃ phase can be detected in the undoped BST powder. The average crystallite

Table 2 Characteristics of the synthesized BST powders calcined 1 h at 900°C obtained by Rietveld refinement: lattice parameters, crystallite size, microstrain, existing crystalline phases and R-factors (%) of the refinements.

Powder	a (Å)	ϵ_β (nm)	Microstrain $\epsilon \times 10^4$	Crystalline phases	R _{wp} [R _{exp}]
Undoped	3.96768	27	25	c-BST + BC(2.6)	19.2[15.0]
Fe–F codoped	3.96336	77	22	c-BST + BF(1.5)	14.8[9.9]
Co–F codoped	3.96399	96	19	c-BST + BF(1.5)	13.8[11.2]
Ni–F codoped	3.96335	98	18	c-BST + BF(1.2)	13.6[8.9]
Cu–F codoped	3.96232	–	–	c-BST + BF(1.7)	12.8[9.3]

wt. % of (Ba,Sr)CO₃ (BC) and BaF₂ (BF) is given in parentheses

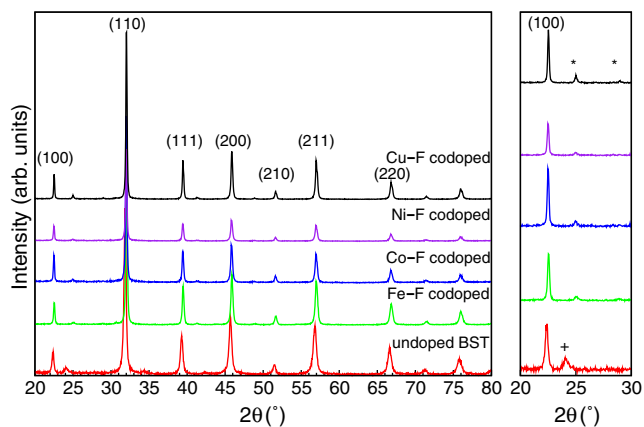


Fig. 2 XRD patterns of the undoped and codoped BST powders calcined at 900°C. + (Ba,Sr)CO₃, * (Ba,Sr)F₂

size is 27 nm with a microstrain of 25×10^{-4} . The calcined codoped powders show no carbonate impurities but small amounts of (Ba,Sr)F₂ (1–2 wt.%) as a secondary phase. The results of the line broadening analysis indicate larger crystallite sizes in the range

between 75 and 100 nm for the codoped powders which implies an enhanced crystallite growth due to doping. For the Cu-F doped sample no reliable microstructural parameters can be extracted due to small line broadening and the limited resolution of the laboratory diffractometer.

In Fig. 3 the SEM micrographs of the BST powders are presented. As can be seen the powders are highly agglomerated and the agglomerates consist of much smaller primary particles. A mean particle diameter was estimated from the SEM micrographs for all samples by measuring about 50 particles and taking the mean of the measured values. The average D_{SEM} values are given in Table 3. They are in good agreement with the volume-weighted diameters D_{β} . The number of crystallites per SEM particle was calculated according to the relation $[(D_{SEM}/D_{\beta})^3]$ [23]. The number of crystallites per SEM particle for all samples lies in the range 0.7–2.2 which is an indication that the primary particles seen with the SEM are single coherent diffracting domains. To quantify the degree

Fig. 3 SEM micrographs of (a) undoped, (b) Fe-F codoped, (c) Co-F codoped, (d) Ni-F codoped and (e) Cu-F coped BST powders calcined at 900°C

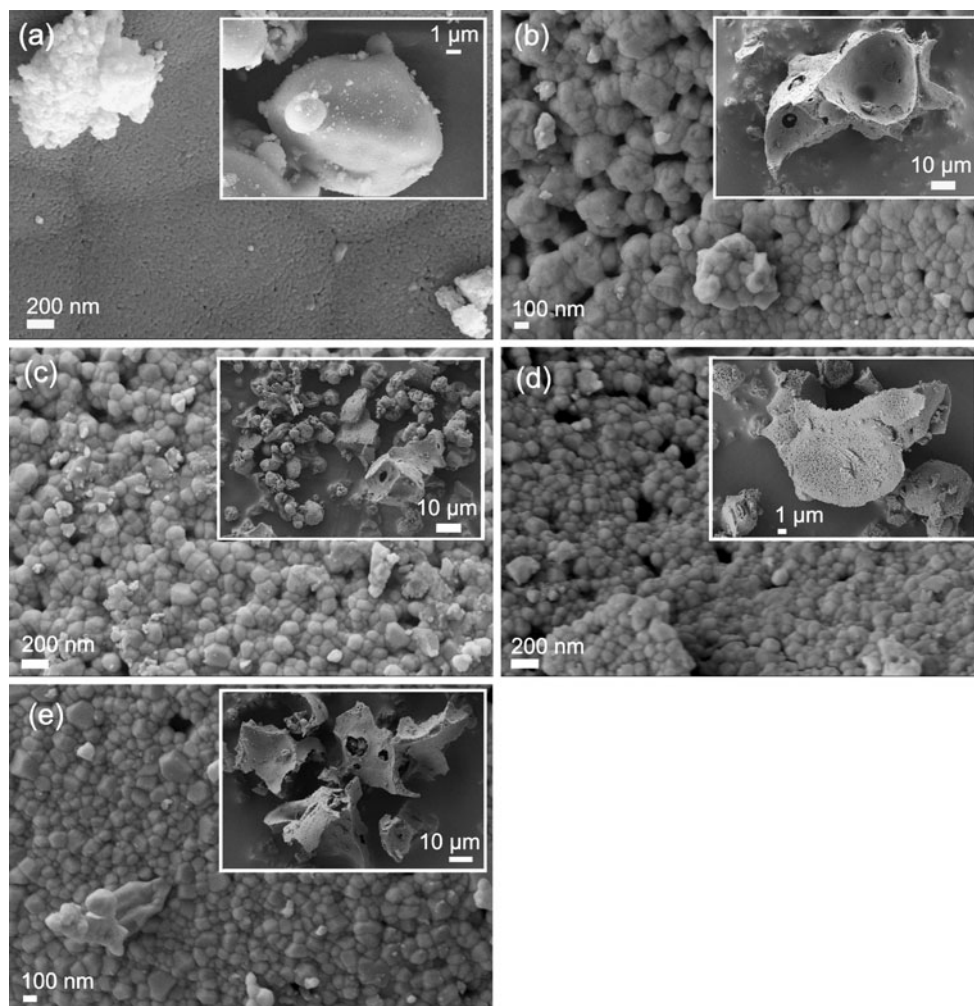


Table 3 Observed surface areas (S_{BET}), mean BET particle diameter D_{BET} , mean SEM particle diameter (D_{SEM}) and number of crystallites per SEM and BET particles ($D_{\text{SEM}}^3/D_{\beta}^3 \cdot D_{\text{BET}}^3/D_{\beta}^3$) of the calcined BST powders.

Powder	D_{SEM} (nm)	$D_{\text{SEM}}^3/D_{\beta}^3$	S_{BET} (m ² /g)	D_{BET} (nm)	$D_{\text{BET}}^3/D_{\beta}^3$
Undoped	–	–	19.91	53	3
Fe–F codoped	133	2.2	3.02	349	39
Co–F codoped	145	1.5	2.32	455	45
Ni–F codoped	117	0.7	2.24	471	47
Cu–F codoped	130	–	2.04	517	–

Assuming spherical crystallites the average diameters (D_{β}) were derived from the apparent crystallite sizes ϵ_{β} according to the relation $D_{\beta} = 4/3\epsilon_{\beta}$

of agglomeration of the calcined powders the specific surface areas (S_{BET}) were measured and are summarized in Table 3. Assuming spherical particles, a mean equivalent grain diameter can be estimated using the relation $D_{\text{BET}} = 6 \times 10^3 / \rho S_{\text{BET}}$, where ρ is the theoretical density of BST ($\rho = 5.69 \text{ g/cm}^3$, the theoretical density of each BST powder was calculated from the refined x-ray lattice parameters), S_{BET} is expressed in m^2/g^{-1} and D_{BET} in nm. The calculated D_{BET} values are listed in Table 3. The D_{BET} value for the undoped powder has the same order of magnitude as the x-ray diffraction diameters whereas the codoped powders exhibit much larger D_{BET} values. If one calculates the average number of crystallites agglomerated within a grain $[(D_{\text{BET}}/D_{\beta})^3]$ the high numbers between 39 and 47 for the doped powders are clearly evident. This suggests that the agglomerates seen in the SEM are rather dense with distinct sinter necks and closed pores. This is in contrast with the undoped BST sample where the average number of crystallites agglomerated within a grain is about 3. Therefore the agglomerates of this sample are porous with open pores.

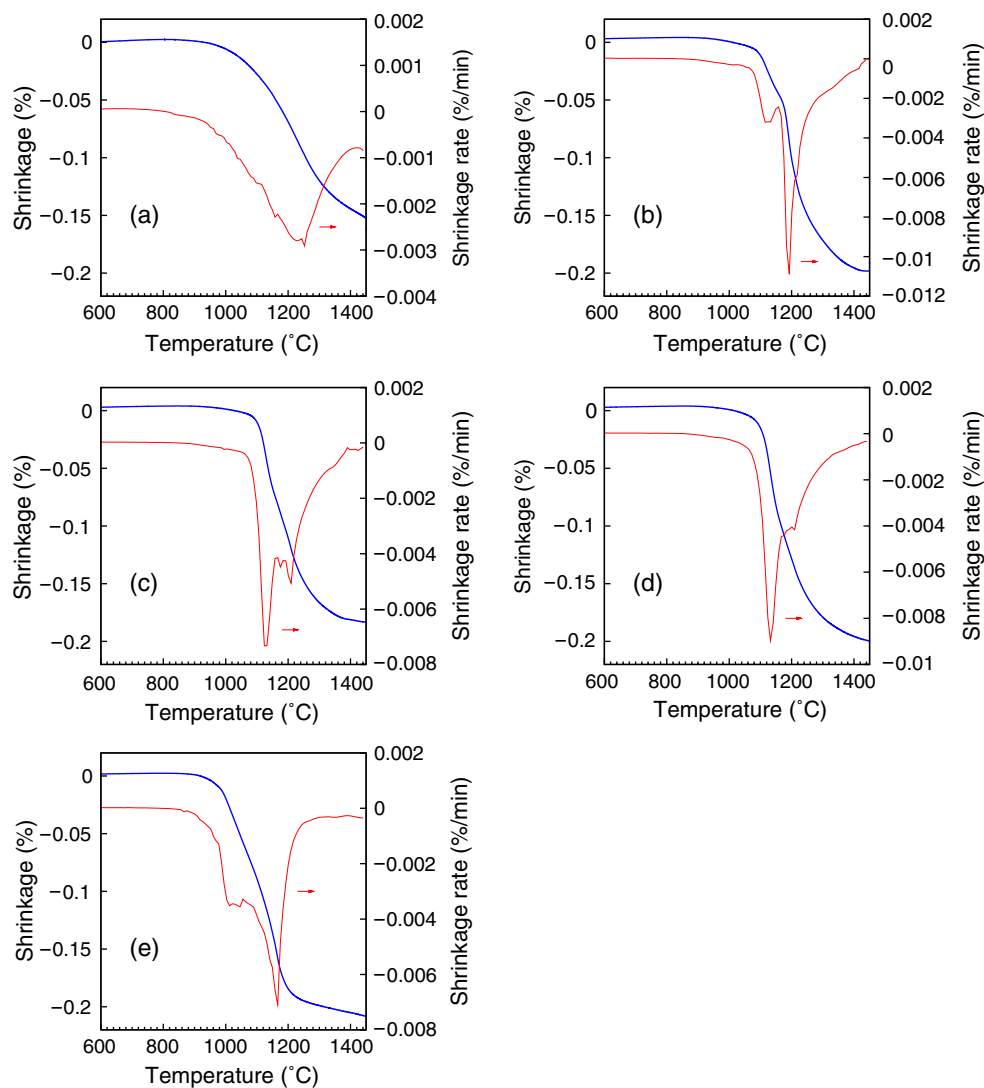
Sintering The effect of the codoping elements on the densification behaviour of BST powder calcined for 1 h at 900°C is reported in Fig. 4. Undoped BST exhibits a one-step sintering behaviour corresponding to a broad minima at approximately 1240°C in the shrinkage rate curve. After a temperature of 1450°C the sintering of the sample is still not completed. The codoped powders show a completely different densification behaviour. Here, a two-step sintering mechanism can be observed. The onset of sintering is shifted to lower temperatures with higher shrinkage rates. At 1450°C sintering is almost completed. The minima of the first step is located between 1020 and 1120°C and the second falls within a range of 1180–1240°C. From the dilatometer curves it can be concluded that codoping enhances the sinter activity of BST powder. This corresponds to the higher observed crystallite sizes and agglomeration as described in the last paragraph.

Chemical analysis Table 4 shows the results of the chemical analysis of the undoped and doped BST powders and corresponding calcined pastes. These results confirm the intended amounts of barium, strontium, titanium and the metal elements. The amount of fluorine in all doped powders is lower than the intended stoichiometry. One reason for the fluorine loss may be the reaction of fluorine with water which is formed during the decomposition process of the metalorganic precursor to gaseous HF at higher temperatures. The amount of fluorine in the calcined screen-printing pastes is also summarized in Table 4. It is evident that the loss of fluorine of the pastes after sintering at 1200°C is higher than the fluorine loss of the pure powders. The fluorine concentrations of the calcined pastes should be comparable to the actual fluorine content of the sintered thick-films because the pastes and thick-films were thermally treated under the same experimental conditions. In addition to the higher sintering temperature of 1200°C another possible reason for this larger fluorine loss may be the additional released water during the decomposition reaction of the organic constituents of the screen-printing paste. Wang [24] and Endo [25] reported that BaTiO₃ doped with F or LiF exothermically decomposed into BaTiO₃ and F₂ gas near 650°C in untreated air. Makovec [26] observed that the majority of the fluorine left the F-doped BaTiO₃ after sintering at 1360°C in untreated air, while half of the fluorine remained in the samples sintered in dried air.

3.2 Characterization of the thick-films

Morphology of the thick-films Figure 5 shows SEM micrographs of fracture surfaces of thick-films sintered at 1200°C for 1 h. It can be seen that the films are not dense with a large porosity and a thickness between 2 and 5 μm. The grain size of undoped, Fe–F and Ni–F codoped thick-films is approximately 200 nm. As can be seen in Fig. 5(c) the Co–F codoped thick-film exhibits a larger grain size of about 400–500 nm compared to the undoped, Fe–F and Ni–F codoped. The crystallite

Fig. 4 Shrinkage and shrinkage rate of (a) undoped, (b) Fe–F codoped, (c) Co–F codoped, (d) Ni–F codoped and (e) Cu–F codoped BST powders calcined at 900°C



growth is most pronounced for the Cu–F codoped sample. These thick-films have the largest grain sizes in the range between 500 and 1 μm (Fig. 5(e)). The x-ray diffraction patterns of the thick-films (not shown here) confirm that no secondary phases have been formed. Additionally, no more carbonate phases and $(\text{Ba,Sr})\text{F}_2$ can be detected in the films.

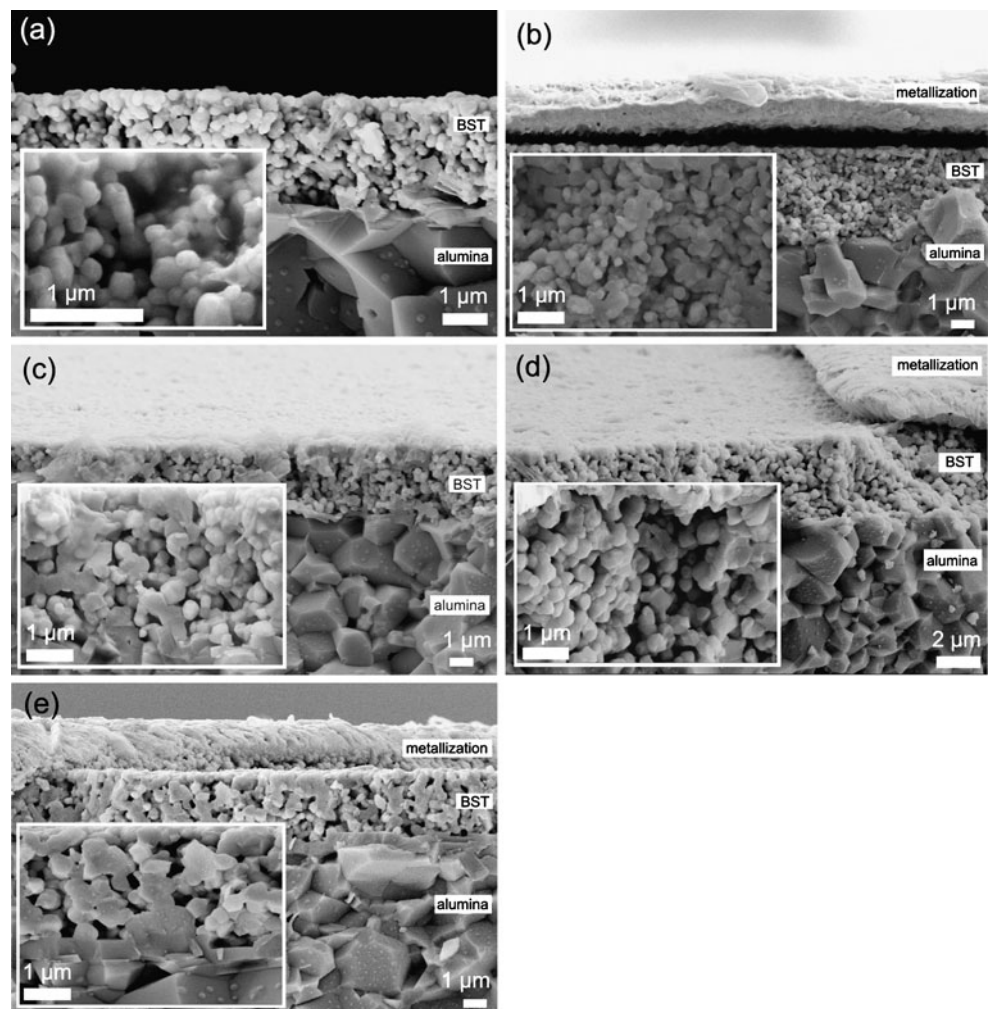
Dielectric properties Figure 6 shows the relative permittivity and the dielectric loss of the undoped and

doped thick-films measured at room temperature as a function of frequency from 5 to 30 GHz in the untuned state. Due to the high relative permittivity of the Cu–F codoped thick-film its dielectric loss can not be reliably extracted from the measurement above 15 GHz. Except for the Ni-doped thick-film the permittivity of the doped thick-films is larger than that of the undoped thick-film. All doped thick-films exhibit a lower dielectric loss compared to that of the undoped thick-film. It is known that the value of the dielectric

Table 4 Results of the chemical analysis (XRF and Titration) of BST powders calcined at 900°C and of the fluorine content of corresponding pastes sintered at 1200°C.

Sample name	Molar composition relative to BST								
	Ba	Sr	Ti	Fe	Co	Ni	Cu	F(powder)	F(paste)
Undoped	0.59	0.39	0.97	–	–	–	–	–	–
Fe–F codoped	0.60	0.40	0.98	0.010	–	–	–	0.067	0.014
Co–F codoped	0.60	0.40	0.98	–	0.010	–	–	0.077	0.021
Ni–F codoped	0.60	0.40	0.98	–	–	0.010	–	0.066	0.023
Cu–F codoped	0.60	0.40	0.98	–	–	–	0.0099	0.068	0.016

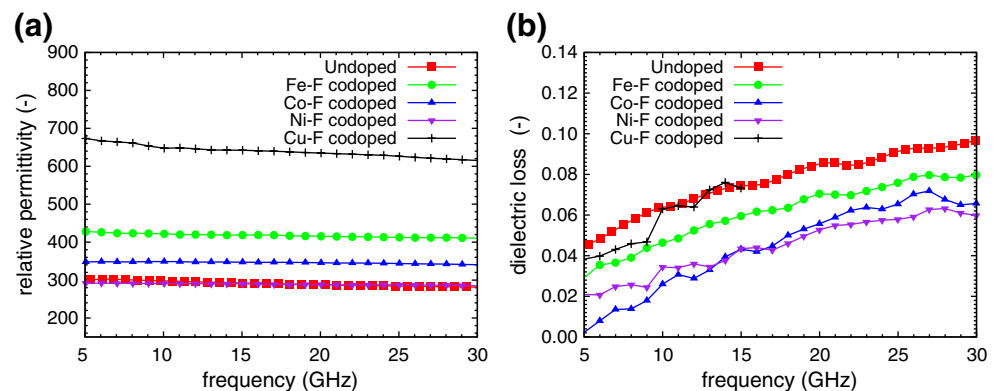
Fig. 5 SEM micrographs of undoped (a), Fe–F codoped (b), Co–F codoped (c), Ni–F codoped (d) and Cu–F codoped (e) BST thick-films



constant of ferroelectric films is strongly affected by microstructure, grain size and doping elements [27]. On the one hand, a larger grain size results in a larger polarization. Hence, higher values of the dielectric constant are expected for materials with larger grain size [28]. On the other hand, acceptor dopants like Fe^{3+} ions and the induced oxygen vacancies construct a strong

internal bias field, which degrades the polarization of the material [29]. Paul [29] reported the dielectric properties of thick-films doped with different amounts of Fe^{3+} and thick-films codoped with Fe–F. In this work the highest dielectric constant was observed for the Fe–F codoped thick-film, whereas pure Fe-doping results in a decreased dielectric constant compared to

Fig. 6 Untuned dielectric properties of the undoped and codoped thick-films. (a) relative permittivity and (b) dielectric losses



that of the undoped thick-film. It was proposed that the fluorine ions occupy the oxygen vacancies, which were generated by the Fe-doping. Consequently the internal field probably decreases and therefore the dielectric constant is increased. We believe that the higher permittivity of the Cu–F and Co–F codoped thick-films is mainly due to the larger grain size of these samples which is a result of the enhanced crystallite growth during sintering in the presence of these dopants. For the Fe–F and Ni–F codoped samples it seems that doping has a major impact on the permittivity because these thick-films show comparable grain sizes as the undoped film (see Fig. 5). However the Curie point of the doped thick-films was not determined in this work. For improving the interpretation and better understanding of the doping effect, more characterization methods particularly a direct verification of the structural incorporation of fluorine in the ceramic BST films are necessary.

Furthermore, it has been reported that Fe^{2+} , Fe^{3+} , Co^{2+} , Co^{3+} , Mn^{2+} , Mn^{3+} , Ni^{2+} , Mg^{2+} , Al^{3+} , Ga^{3+} , In^{3+} , Cr^{3+} , and Sc^{3+} ions, which can occupy the B site of the perovskite structure as acceptor dopants, can lower the dielectric loss [9, 30, 31]. Acceptor-type dopants can prevent the reduction of Ti^{4+} to Ti^{3+} by neutralizing the donor action of the oxygen vacancies. Because the electrons resulting from the generation of oxygen vacancies can hop between different titanium ions and provide a mechanism for dielectric losses, the compensation for oxygen vacancy with the correct amount of acceptor dopant such as Fe^{3+} , Co^{2+} , Ni^{2+} , Cu^{2+} should in theory help to lower the loss tangent. It was previously reported that fluorine acts as a donor dopant [13]. It can prevent the influence of oxygen vacancies on the dielectric loss without building new defects in the crystal structure and enhances the dielectric properties of the doped thick-films. The differences of dielectric loss between the codoped thick-films are not clearly understood yet and further investigations are necessary.

Tunability The effective dielectric tunability $\tau(E)$ is defined in Eq. 1, where $\varepsilon_r(E = 0)$ is the relative permittivity in the absence of a dc bias field E and $\varepsilon_r(E)$ is the permittivity in the presence of a bias field.

$$\tau(E) = \frac{\Delta\varepsilon_r(E)}{\varepsilon_r(E = 0)} = \frac{\varepsilon_r(E = 0) - \varepsilon_r(E)}{\varepsilon_r(E = 0)} \quad (1)$$

The tunability $\tau(E)$ of the undoped and doped thick-films as a function of the effective tuning field strength measured at 10 GHz is shown in Fig. 7. The tunabilities $\tau(E = 5\text{V}/\mu\text{m})$ of Cu–F codoped, Fe–F codoped, undoped, Ni–F codoped, Co–F codoped thick-films mea-

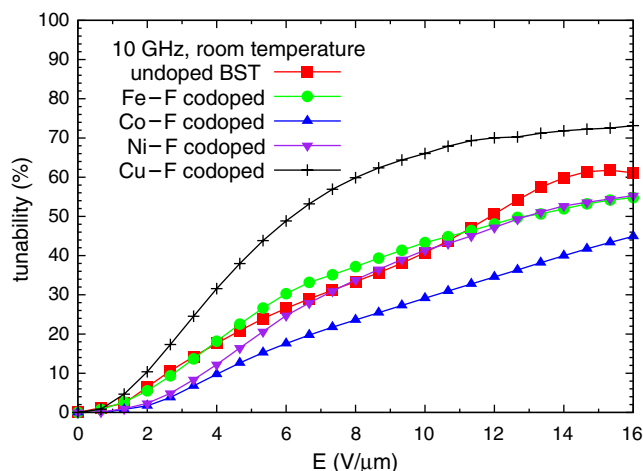


Fig. 7 The tunability of the undoped and codoped thick-film in function of effective tuning field strength at 5 GHz

sured at 10 GHz at room temperature are 41%, 25%, 22%, 18% and 14%, respectively. This indicates that the Cu–F and Fe–F codoped thick-films have a higher tunability than the undoped films while the tunability of the Ni–F codoped and Co–F codoped thick-films are smaller than that of the undoped film at the same bias field E . In general, the higher the dielectric constant, the greater a $\Delta\varepsilon$ can be achieved for a given voltage. Considering the greater permittivity of Cu–F codoped and Fe–F codoped thick-films shown in Fig. 6, their much higher tunability compared to the other thick-films at the same dc bias field is reasonable. On the contrary, the tunability of Ni–F codoped and Co–F codoped thick-films is smaller than the undoped thick-film in spite of their moderate permittivity. The reduction of tunability in Co-doped BST ceramics [32] and in Ni-doped BST thin films [15] has also been reported.

4 Conclusions

Undoped, Fe–F codoped, Co–F codoped, Ni–F codoped and Cu–F codoped $\text{Ba}_{0.6}\text{Sr}_{0.4}\text{TiO}_3$ powders have been prepared and characterized. The synthesis of the powders was carried out through a sol-gel process and spray-drying of the sol. Different acceptor-dopants like Fe, Co, Ni, Cu have been quantitatively incorporated according to the XRF analysis. However, the measured amount of fluorine is lower than the nominal amount. The thermal gravimetric analysis revealed that the codoped precursors show a different decomposition behaviour compared to that of the undoped. The x-ray diffraction patterns of the ceramic powders after calcination for 1 h at 900°C showed

the formation of a secondary phase (< 2 wt.%) in undoped and codoped samples. The results of the line broadening analysis indicated larger crystallite sizes for codoped powders. The increase of crystallite size was also confirmed by the SEM micrographs and BET surface analysis. The dilatometry measurement showed a two-step sintering behaviour and higher sinter activity for codoped powders.

The morphology of the thick-films was investigated by SEM micrographs of the fracture surface. Cu–F codoped thick-films showed the largest grain size of all films. The permittivity of the thick-films was almost frequency-independent, aside from the slight increase of permittivity of the Cu–F codoped thick-film with increasing frequency. The codoped samples have a higher permittivity than the undoped. It is proposed that the grain growth due to doping and additional fluoridation have a positive influence on the permittivity. Furthermore, the dielectric loss of the thick-films increased with increasing frequency and the codoped thick-films showed smaller values compared to that of the undoped. Cu–F thick-films exhibit the highest tunability due to their highest permittivity. The reduction of tunability with Ni–F codoping and Co–F codoping can also be observed.

The investigated materials show promising characteristics for tunable radio frequency applications. However, for an application of such doped thick films in future tunable components the dielectric properties of the ceramic material itself, the processing, the integration of the ceramic film in conjunction with the specific requirements of each application have to be taken into account.

Acknowledgements This work was supported in part by the German Research Foundation (DFG) Research Training Group 1037 Tunable Integrated Components in Microwave technology and Optics (TICMO).

References

- R. Babbitt, T. Koscica, W. Drach, L. Didomenico, Ferroelectric phase shifters and their performance in microwave phased array antennas. *Integr. Ferroelectr.* **8**(1–2), 65–76 (1995)
- W. Wilber, W. Drach, T. Koscica, R. Babbitt, L. Sengupta, S. Sengupta, Fabrication and performance of coplanar ferroelectric phase shifter. *Integr. Ferroelectr.* **19**(1–4), 149–158 (1998)
- A. Tombak, J.P. Maria, F.T. Ayguavives, Z. Jin, G.T. Stauf, A.I. Kingon, A. Mortazawi, Voltage-controlled RF filters employing thin-film barium-strontium-titanate tunable capacitors. *IEEE Trans. Microwave Theor. Tech.* **51**(2), 462–467 (2003)
- A. Jamil, T.S. Kalkur, N. Cramer, Tunable ferroelectric capacitor-based voltage-controlled oscillator. *IEEE Trans. Ultrason. Ferroelectr. Freq. Control* **54**(2), 222–226 (2007)
- F. Zimmermann, M. Voigts, W. Menesklou, E. Ivers-Tiffée, Ba_{0.6}Sr_{0.4}TiO₃ and BaZr_{0.3}Ti_{0.7}O₃ thick films as tunable microwave dielectrics. *J. Eur. Ceram. Soc.* **24**(6), 1729–1733 (2004)
- P. Scheele, A. Giere, Y. Zheng, F. Goelden, R. Jakoby, Modeling and applications of ferroelectric-thick film devices with resistive electrodes for linearity-improvement and tuning-voltage reduction. *IEEE Trans. Microwave Theor. Tech.* **55**(2), 383–390 (2007)
- Y. Zheng, A. Hristov, A. Giere, R. Jakoby, Suppression of harmonic radiation of tunable pifa by thick-film bst varactor loading, in *IEEE MTT-S International Microwave Symposium Digest*, (2008) pp. 959–962
- M.W. Cole, P.C. Joshi, M.H. Ervin, M.C. Wood, R.L. Pfeffer, The influence of Mg doping on the materials properties of Ba_{1-x}Sr_xTiO₃ thin films for tunable device applications. *Thin Solid Films* **374**(1), 34–41 (2000)
- P.C. Joshi, M.W. Cole, Mg-doped Ba_{0.6}Sr_{0.4}TiO₃ thin films for tunable microwave applications. *Appl. Phys. Lett.* **77**(2), 289–291 (2000)
- J.W. Liou, B.S. Chiou, Dielectric characteristics of doped Ba_{1-x}Sr_xTiO₃ at the paraelectric state. *Mater. Chem. Phys.* **51**(1), 59–63 (1997)
- S.B. Herner, F.A. Selmi, V.V. Varadan, V.K. Varadan, The effect of various dopants on the dielectric properties of barium strontium titanate. *Mater. Lett.* **15**(5–6), 317–324 (1993)
- J. Gong, J. Cheng, W. Zhu, S. Yu, W. Wu, Z. Meng, Improvement in dielectric and tunable properties of Fe-doped Ba_{0.6}Sr_{0.4}TiO₃ thin films grown by pulsed-laser deposition. *IEEE Trans. Ultrason. Ferroelectr. Freq. Control* **54**(12), 2579–2582 (2007)
- F. Paul, A. Giere, W. Menesklou, J.R. Binder, P. Scheele, R. Jakoby, J. Hausselt, Influence of Fe-F-co-doping on the dielectric properties of Ba_{0.6}Sr_{0.4}TiO₃ thick-films. *Int. J. Mater. Res.* **99**(10), 1119–1128 (2008)
- L.N. Gao, S.N. Song, J.W. Zhai, X. Yao, Improvement of dielectric properties of graded co-doped (Ba_{0.7}Sr_{0.3}) TiO₃ thin films fabricated by sol-gel method. *Ferroelectrics* **357**, 142–147 (2007)
- M.H. Lim, H.S. Kim, N.Y. Kim, H.G. Kim, I.D. Kim, S.E. Moon, M.H. Kwak, H.C. Ryu, S.J. Lee, Frequency and voltage dependent dielectric properties of Ni-doped Ba_{0.6}Sr_{0.4}TiO₃ thin films. *J. Electroceramics* **13**(1–3), 239–243 (2004)
- A. Giere, P. Scheele, Y. Zheng, R. Jakoby, Characterization of the field-dependent permittivity of nonlinear ferroelectric films using tunable coplanar lines. *IEEE Microw. Wirel. Compon. Lett.* **17**(6), 442–444 (2007)
- D. Hennings, G. Rosenstein, H. Schreinemacher, Hydrothermal preparation of barium titanate from barium-titanium acetate gel precursors. *J. Eur. Ceram. Soc.* **8**(2), 107–115 (1991)
- F. Paul, J.R. Binder, H. Gesswein, H.-J. Ritzhaupt-Kleissl, J. Hausselt, Synthesis of doped Ba_{0.6}Sr_{0.4}TiO₃ ceramic powder via a sol-freeze-granulation and freeze-drying process. *Ceram. Int.* **35**(1), 479–486 (2009)
- V. Somani, S.J. Kalita, Synthesis and characterization of nanocrystalline barium strontium titanate powder via sol-gel processing. *J. Electroceramics* **18**(1–2), 57–65 (2007)
- C.L. Mao, X.L. Dong, T. Zeng, G.S. Wang, S. Chen, Formation and control of mechanism for the preparation of ultra-fine barium strontium titanate powders by the citrate precursor method. *Mater. Res. Bull.* **42**(9), 1602–1610 (2007)

21. J. Rodriguez-Caraval, Recent advances in structure determination by neutron powder diffraction. *Phys., B* **192**, 55–69 (1993)
22. J. Rodriguez-Carvajal, T. Roisinel, Line broadening analysis using fullprof: determination of microstructural parameters. *Mat. Sci. Forum* **443–444**, 123–126 (2004)
23. N. Audebrand, C. Bourgel, D. Louër, Ex-oxalate magnesium oxide, a strain-free nanopowder studied with diffraction line profile analysis. *Powder Diffr.* **21**(3), 190–199 (2006)
24. S.F. Wang, T.C.K. Yang, W. Huebner, J.P. Chu, Liquid-phase sintering and chemical inhomogeneity in the BaTiO₃-BaCO₃-LiF system. *J. Mater. Res.* **15**(2), 407–416 (2000)
25. T. Endo, T. Kobayashi, T. Sato, M. Shimada, High pressure synthesis and electrical properties of BaTiO_{3-x}F_x. *J. Mater. Res.* **25**(1), 619–623 (1990)
26. D. Makovec, M. Drogenik, J. Baker, Fluorine as a donor dopant in barium titanate ceramics. *J. Am. Ceram. Soc.* **86**(3), 495–500 (2003)
27. A. Giere, X. Zhou, F. Paul, M. Sazegar, Y. Zheng, H. Maune, J.R. Binder, R. Jakoby, Barium strontium titanate thick-films: dependency between dielectric performance and their morphology. *Frequenz* **62**(3–4), 47–51 (2008)
28. M.W. Cole, C. Hubbard, E. Ngo, M. Ervin, M. Wood, R.G. Geyer, Structure-property relationships in pure and acceptor-doped Ba_{1-x}Sr_xTiO₃ thin films for tunable microwave device applications. *J. Appl. Phys.* **92**(1), 475–483 (2002)
29. F. Paul, *Dotierte Ba_{0,6}Sr_{0,4}TiO₃-Dickschichten als steuerbare Dielektrika: Pulversynthese und dielektrische Eigenschaften*, PhD thesis, Albert-Ludwigs-Universität Freiburg im Breisgau (2006)
30. T.B. Weston, A.H. Webster, V.M. McNamara, Lead zirconate-lead titanate piezoelectric ceramics with iron oxide additions. *J. Am. Ceram. Soc.* **52**(5), 253–257 (1969)
31. V.K. Varadan, D.K. Ghodgaonkar, V.V. Varadan, J.F. Kelly, P. Glikerdas, Ceramic phase shifters for electronically steerable antenna systems. *Microw. J.* **35**(1), 116–127 (1992)
32. R.H. Liang, X.L. Dong, P.H. Xiang, H.D. Li, Effect of Co₂O₃ doping on the dielectric and tunable properties of Ba_{0,6}Sr_{0,4}TiO₃ ceramics. *Jpn. J. Appl. Phys. Part 1, Regular Papers Short Notes & Review Papers* **43**(1), 201–204 (2004)